Published in final edited form as:

J Immunol. 2021 July 01; 207(1): 221–233. doi:10.4049/jimmunol.2001276.

Novel Role for Macrophage Galactose-type Lectin-1 to Regulate Innate Immunity against *Mycobacterium tuberculosis*

Kubra F. Naqvi[*], **Matthew B. Huante**[*], **Tais B. Saito**[†,‡], **Mark A. Endsley**[*], **Benjamin B. Gelman**[†], **Janice J. Endsley**[*]

[*]Department of Microbiology and Immunology, University of Texas Medical Branch, Galveston, TX, 77555, USA

[†]Department of Pathology, University of Texas Medical Branch, Galveston, TX, 77555, USA.

[‡]Now affiliated with the Vector-Pathogen-Host Interaction Unit, Laboratory of Bacteriology, Rocky Mountain Laboratories, National Institute of Allergy and Infectious Diseases, National Institutes of Health, Hamilton, Montana 59840, USA.

Abstract

Tuberculosis (TB) caused by infection with *Mycobacterium tuberculosis* (*Mtb)* is characterized by inflammatory pathology and poorly understood mechanisms of innate immunity. Pattern recognition receptors (PRR), expressed on the surface of macrophages, determine the balance of inflammatory and antimicrobial functions that influence disease outcome. Carbohydrate moieties displayed by mycobacteria can serve as PRR ligands for some members of the C-type lectin receptor (CLR) family; interactions that mediate a variety of incompletely understood immune outcomes. This work identifies a novel role for the CLR Macrophage Galactose-type Lectin-1 (MGL-1) in a mouse model (C57BL/6 and MGL-1$^{-/-}$) of experimental TB. Murine macrophages upregulated MGL-1 following *in vitro* exposure to *Mtb,* while MGL^{+} cells accumulated at sites of mycobacteria-driven inflammation in the lung. Pulmonary macrophages from MGL-1-deficient mice displayed increased production of pro-inflammatory cytokines (IL-1β, IL-6 and IFN-γ) that was associated with greater lipid accumulation, following *Mtb* infection. Surprisingly for a CLR, we also observed MGL-1-dependent anti-mycobacterial activity as evidenced by greater *Mtb* proliferation in BMDM, and the lung, of MGL-1 deficient mice. Differential transcriptome analysis further revealed that loss of MGL-1 perturbs activation of various genes involved in the regulation of inflammation and lipid metabolism in the setting of *Mtb* infection. These results identify MGL-1 signaling as an important mechanism that regulates innate immunity against *Mtb* and indicate potential for the MGL pathway as a novel therapeutic target for anti-TB immunity.

Keywords

Tuberculosis; C type lectin receptor; Macrophage Galactose-type Lectin (MGL); inflammation; innate immunity

Corresponding author: jjendsle@utmb.edu (JJE).

RNASeq Database Submission: The data discussed in this publication have been deposited in NCBI's Gene Expression Omnibus (Edgar et al., 2002) and are accessible through GEO Series accession number GSE168486 (https://www.ncbi.nlm.nih.gov/geo/query/acc.cgi?acc=GSE168486).

Introduction

Mycobacterium tuberculosis (*Mtb*), the etiologic agent of pulmonary TB, is the leading cause of death by a single infectious agent. In 2019 alone, there were 1.3 million deaths due to TB and 10 million new reported cases worldwide (1). Disruptions to healthcare and economies in the wake of the unfolding Covid-19 pandemic are further predicted to set TB progress back at least 5 to 8 years (2). Efforts to more fully characterize the complex nature of TB immunity and disease progression are essential to guide development of preventative and therapeutic interventions.

Innate immune responses, especially by macrophages and dendritic cells, play an important role in directing pathogen-specific immunity and determining disease outcomes. Upon initial inhalation of *Mtb* into the alveolar space, local macrophages recognize and internalize the bacilli, triggering an early innate immune response that serves to either control or harbor infection (3–5). Macrophages display a great deal of heterogeneity during the course of disease that can produce both pro-inflammatory and anti-inflammatory environmental milieu to promote pathogen clearance or permissiveness, respectively (6, 7). The activation and reprogramming of macrophages by *Mtb* occurs in part through initial interaction of mycobacterial components with pattern recognition receptors (PRR) which can internalize or bind *Mtb* (8). PRR signaling through toll-like receptors (TLR), NOD-like receptors (NLR), and CLRs have all been associated with *Mtb* infection and are capable of co-signaling to dictate overall immune outcomes and intracellular fate of the bacteria (9).

CLRs comprise an important family of carbohydrate recognizing PRRs, which have been shown to bind, internalize, and control *Mtb* within macrophages (8). The surface of *Mtb* includes a diverse repertoire of carbohydrate residues and glycolipids which can be recognized and bound in a calcium dependent manner by CLRs (10). The host PRR receptors and the respective interactions with these molecular patterns of *Mtb* that determine immune outcomes are incompletely characterized. To date, roles for CLRs during *Mtb* infection has been shown to include entry into macrophages, as demonstrated for the Mannose Receptor (MMR) and DC-SIGN (11, 12), immune activation as shown for Dectin 1 and Dectin 2 (13, 14), and granuloma formation as shown for Macrophage-inducible C-type lectin (Mincle) (15). CLRs expressed on alveolar macrophages (MMR and DC-SIGN) recognize mannose containing mycobacterial membrane molecules including arabinomannan, lipomannan, and Man-Lam, leading to internalization and an anti-inflammatory immune response through increased IL-10 secretion (16, 17). Many CLRs recognize redundant carbohydrate motifs and are capable of crosstalk with other PRRs, resulting in compensatory signaling during receptor impairment (18–20). Therefore, understanding the broad spectrum of macrophage CLR functions can lead to improved insight into antimycobacterial innate immunity and TB immunopathogenesis.

Macrophage Galactose-type lectin (MGL,CD301,CLEC10A) is a galactose binding CLR expressed on alternatively activated macrophages and DCs (21). Unlike other CLRs, MGL appears to have a non-redundant specificity for N-acetylgalactosamine residues (22). While human cells express a single transmembrane receptor, mice express two homologous

receptors, MGL-1 and MGL-2 (23). The immune role for MGL, to date, has been mostly characterized by anti-tumor immunity in which MGL can recognize Tn-MUC-1, an aberrantly glycosylated host protein associated with many carcinomas (24, 25). The result of this interaction is immune dampening by increased IL-10 and IL-4 production. In one report, MGL signaling was effectively exploited as an anti-tumor therapy using glycan mimetics against ovarian cancer (26). MGL has also been shown to bind bacterial pathogens including *Klebsiella pneumonia, Neisseria gonorrhea,* and *Bordetella pertussis* (27–29). In a murine model of *Klebsiella pneumonia*, deficiency of MGL-1 resulted in neutrophilic pneumonia and hyperinflammatory lung pathology (27). These studies indicate the potential for MGL pathways in innate immunity of diverse infectious and non-communicable diseases, however, a role in immune recognition of mycobacteria has not been described.

The results of the current investigations identify a new immune role for MGL in the protective innate immune response to *Mtb* infection. Our findings show that MGL-1 is activated by exposure to *Mtb* and is abundantly expressed at sites of pulmonary TB. Deficiency of MGL-1 leads to exacerbated inflammation that is independent of bacterial proliferation, accumulation of lipids in pulmonary macrophages, and increases in lung mycobacterial burden. Together these findings suggest that MGL-1 is an important PRR system in the host response to *Mtb* and may be a target for host directed approaches to reduce damaging inflammation and bacterial proliferation.

Materials and Methods

Mice and cell lines

Experiments were performed using C57BL/6 and *Clec10a* deficient (MGL-$1^{-/-}$) or WT littermates obtained or generated from breeder pairs from The Jackson Laboratory. Cryopreserved B6.129- *Clec10a*^{tm1Hed}/J embryos (MGL-$1^{+/-}$) were recovered from The Jackson Laboratory and breeding colonies were maintained by the transgenic mouse core (University of Texas Medical Branch) for all *in vivo* and *in vitro* assays. All experimental protocols involving use of mice were approved by the University of Texas Medical Branch Institutional Animal Care and Use Committee protocol #1501001A. The RAW 264.7 murine macrophage cell line was obtained from the American Type Culture Collection and cultivated using DMEM media supplemented with 10% FBS, 1% Pen Strep, 1% L-glutamine, and 1% non-essential amino acids.

Animal infections

Mtb H37Rv (ATCC 27294) was propagated from a growth stock in Middlebrook 7H9 media and used to deliver 10^2 CFU of *Mtb* for pulmonary infections. The required inoculum volume of bacterial suspension was diluted in PBS and delivered by intranasal route in 50μL (25μL/ nare). Following 2, 4, 6 or 8 weeks p.i. the right lung (superior, inferior, and post-caval lung lobes) was collected in 1 ml PBS and disrupted using a tissue homogenizer pestle (Corning). CFU enumeration of disrupted lung was performed with limiting dilution and growth on 7H11 agar plates as described (30). Remaining lung supernatant was centrifuged at 3,000 rpm for 10 minutes to clarify and preserved at −80°C for downstream

analysis. The left lung lobe was fixed in 10% buffered formalin for subsequent histology and immunohistochemistry (IHC) analysis.

In vitro macrophage assays

The RAW 264.7 murine macrophage cell line was cultivated and plated in tissue cultured treated 24-well plates at 1×10^6 cells per well. Cells were then stimulated with dexamethasone (1μM) as a positive control to activate MGL, or infected with 10 MOI *Mtb* H37Rv for 24, 48, or 72 hours. Flow cytometric analysis was used to determine MGL-1, MGL-2, and MMR surface expression of RAW cells. Cells were harvested and washed with PBS followed by staining with the Near Infrared (NIR) viability marker (Thermo Fisher). Non-specific interactions were reduced by a 5 minute incubation with Fc Block (BD Biosciences). Samples were incubated with surface markers specific to MGL-1 (PE, Biolegend), MGL-2 (APC, Biolegend), and MMR (BV650, Biolegend) for 1 hour, washed twice with FACS buffer (PBS supplemented with 1% HI FBS and 0.05% sodium azide), and fixed for 48 hours in 4% ultrapure formaldehyde (Polysciences) to inactivate *Mtb*.

Compensation values were determined using the UltraComp compensation bead control (Thermo Fisher) and applied during acquisition and analysis. A minimum of 100,000 events in the live leukocyte gate were acquired on the BD LSR II Fortessa using FACS Diva software. Data analysis was performed using FCS express 6 software. Selection gates were set based on forward and side scatter characteristics and viability, and expression of designated CLRs. The percent expression of selected markers was compared across time points of infection. Additionally, whole cell lysates from RAW cells were collected using 1x RIPA buffer (Cell Signaling) supplemented with a protease inhibitor cocktail (Sigma) and used to perform western blot analysis. Protein concentrations were determined by BCA assay (Thermo Scientific) and 70μg of protein was loaded onto 4–20% SDS-PAGE for electrophoresis followed by transfer to nitrocellulose membranes. Membranes were exposed to primary anti-mouse MGL antibody (Abcam, 1:900) and anti-β-tubulin (Abcam, 1:2000) overnight in 5% milk powder + 1% BSA in TBS blocking buffer. After washing, the membranes were incubated with anti-rabbit or mouse HRP-conjugated antibody (Southern Biotechnology). Protein bands were visualized by SuperSignal West Femto maximum sensitivity substrate (Thermo scientific) and imaged on the chemiluminescent Image Quant (GE).

Bone marrow derived macrophages (BMDM) were generated by harvest of bone marrow from isolated femurs of MGL-$1^{-/-}$ mice or WT littermates by flushing with RPMI supplemented with 10% FBS, 1% Pen Strep, 1% L-glutamine, 1% HEPES and 1% Non-essential amino acids (c-RPMI). Recovered bone marrow cells were seeded at 1×10^6 per well in 24-well plates and macrophages were derived using 50 ng/mL of M-CSF (Stemcell) for five days at 37°C. Following derivation, cells were exposed to 10 MOI of *Mtb* H37Rv for 1, 4, 12, 24, or 72 hours.

Quantitative real-time PCR

Whole cellular RNA was extracted from BMDMs in accordance with the manufacturer's protocol (BioRad Aurum kit) and quantified by nanodrop (Biotek). RNA was reverse

transcribed and used for quantitative real time PCR analysis using an iTaq Universal SYBR green one-step kit (BioRad). Thermal cycling conditions were 50°C for 10 minutes; 95°C for 1 minute; 38 cycles of 95°C for 10 seconds; 60°C for 20 seconds on the Bio-rad CFX96 Real-time PCR system. The primers complementary to *mmgl1, mmgl2, map3k6, creb5, tlr13, chd9, mmp9, cxcr2,* and *actin* sequences were synthesized by IDT. PRIMER sequences as described by (31).

mmgl1 (sense) 5'-AACCTCCAGAACTCAAGGATCG- 3' and (antisense) 5'-AGCTTTACCAGGCTCTTGGGT- 3'.

mmgl2 (sense) 5' CAGAACTTGGAGCGGGAAGAG 3' and (antisense) 5'-TTCTTGTCACCATTTCTCATCTCCT – 3'.

map3k6 (sense) 5'-CGTCGCAAAGGGTAGGCTG-3' and (antisense) 5'-GCCTCTCAGTGTGGTCTACG-3'

creb5 (sense) 5'-GCGCAGCCTTCAGTCTCAT-3' and (antisense) 5'-AGGATCTTCTGCCGTCTTGAT-3'

tlr13 (sense) 5'-GCACCTTCGTCGATCTTCCAA-3' and (antisense) 5'-CCAACTTGACAGAGGCCATTAG-3'

chd9 (sense) 5'-CGTTCCTCTGTGATTGGTTGAAT-3' and (antisense) 5'-GAGGGCAGTTTGATTGGACAA-3'

mmp9 (sense) 5'-CTCGCGGCAAGTCTTCAGAG-3' and (antisense) 5'-CTGGACAGCCAGACACTAAAG-3'

cxcr2 (sense) 5'-GTGCTCCGGTTGTATAAGATGAC-3' and (antisense) 5'-ATGCCCTCTATTCTGCCAGAT-3'

Histopathology and immunohistochemistry

Paraffin-embedded lung sections were serially sectioned (5μm) and stained with hematoxylin and eosin (H&E) by the UTMB surgical pathology core facility. Stained sections were analyzed by light microscopy and scored for specific pathological criteria in a blinded analysis. Additional sections were used to perform IHC staining to detect MGL. A primary rabbit antibody specific for mouse MGL (Abcam) followed by a secondary anti-rabbit IgG AP (Vector) kit was used for the staining protocol. The antibody to murine MGL binds both MGL-1 and MGL-2 and, to date, an antibody that distinguishes between isoforms is not commercially available for IHC. Positive markings were visualized with fast red chromogen (Vector Laboratories) and analyzed by light microscopy.

Macrophage polarization assessment

To determine *in vitro* macrophage polarization bias (M1 vs M2), WT (MGL-$1^{+/+}$) and MGL-$1^{-/-}$ BMDM were infected with 10 MOI *Mtb* H37Rv or mock infection (BSA). Following 24 hours of infection, cells were incubated with surface markers F4/80 (BV510, Biolegend), CD11b (evolve 605, eBioscience), CD80 (BV 711, BD), MMR (BV

650, Biolegend). Following surface staining, cells were permeabilized using a fixation/permeabilization kit (BD cytofix/cytoperm) for intracellular staining of IL-10 (APC, Biolegend), inos (FITC, Miltenyi Biotec), and arginase (eflour 450, Thermo Fisher).

Nitric oxide assay

WT (MGL-$1^{+/+}$) and MGL-$1^{-/-}$ BMDM were infected with 10 MOI *Mtb* H37Rv for 12 and 24 hours. Following infection, supernatants were collected and stored at −80°C until use for subsequent assays. Supernatants were inactivated by γ-irradiation as described (30) and nitrite concentrations were quantified using the Measure-iT High-sensitivity Nitrite Assay Kit (Invitrogen) as an estimate of nitric oxide (NO). The kit was used following manufacturer instructions and fluorescent intensity was measured using the Synergy H1 (Biotek) plate reader. Nitrite concentrations were extrapolated using a linear regression of standards.

Phagocytosis assay

A 1 mL aliquot of *Mtb* culture (OD 0.5) was stained with 15uM of CFSE for 45 minutes at 37°C with periodic agitation. Cells were washed with PBS to remove residual stain and isolated BMDMs were infected at 20 MOI for 2 hours. Macrophages were washed with PBS to remove extracellular bacteria and dissociated from the culture plate. Cells were fixed with 4% ultra-pure formaldehyde for 48 hours and acquired on a BD Fortessa cytometer. Cells were selected based on forward and side scatter characteristics and the MFI of FITC positive cells was determined using FCS Express 6 flow cytometry software analysis (DeNovo Software).

Cytokine and chemokine quantification

Homogenized lung supernatants were inactivated by exposure to 5 MRAD γ-irradiation on dry ice, as described (32). Pathogen inactivation was confirmed by lack of detectable mycobacterial growth following a 3 week culture on 7H11 agar plates. Immune analytes, including cytokines and chemokines, were measured using multiplex magnetic bead ELISA (Bio-rad Bio-plex Pro mouse cytokine 23-plex) and analyzed as described (33).

Flow cytometric assessment of lung macrophage phenotype and leukocyte influx

Total mouse lungs were enzymatically digested with DNase I (Sigma) and collagenase IV (Worthington Biochemical) and homogenized through a 70μm mesh filter. Digested lungs were subjected to three rounds of low speed (60×g for 1 min) centrifugation to remove fibroblasts and debris during isolation of lung leukocytes. Isolated leukocytes were treated with RBC lysis buffer (BD FACS lyse) for 5 minutes. Following wash with PBS, cells were stained with fixable live/dead stain near IR (Invitrogen) for 2 minutes and incubated with Fc block for 5 minutes to reduce non-specific staining. Samples were incubated with surface antibodies suspended in brilliant violet staining buffer (BD) and incubated for 30 minutes at 4°C. Samples were fixed in 4% ultra-pure formaldehyde solution to inactivate *Mtb* and acquired on a BD LSR II Fortessa cytometer. Antibodies included CD301a (PE, Biolegend), CD301b (APC, Biolegend), F4/80 (BV-510, Biolegend), CD11c (PE/dazzle 594, Biolegend), Ly-6G (Pacific Blue, Biolegend), CD3 (FITC, Biolegend), (eVolve 605, eBioscience), CD4

(BUV 496, BD) and CD8 (PE-alexa 647, BioRad). In additional experiments, the expression of MGL-1 by lung compartment macrophage populations was assessed. Disrupted lung tissue was analyzed with multiparameter flow cytometry by using antibodies to surface markers that permit determination of alveolar and interstitial phenotypes. Antibodies used included CD11b (evolve605, Thermo Fisher), CD11c (PE-dazzle 594, Biolegend), CD64 (FITC, Biolegend), Siglec-F (Alexa Fluor 647, BD Biosciences), Mannose Receptor (BV 650, Biolegend), CD301a (PE, Biolegend) and a fixable viability marker (live/dead- near IR, Thermo Fisher).

Lipid body staining

In separate samples, leukocytes from disrupted lung tissue were assessed for intracellular lipid accumulation. Isolated lung cells were stained with fixable live/dead Near IR (Invitrogen) for 2 minutes at RT and washed with PBS. Cells were then re-suspended in Nile red staining solution (Abcam) and incubated for 20 minutes at 37 °C with periodic agitation. Once stained, cells were washed with sterile PBS and fixed with 4% ultra-pure formaldehyde to inactivate *Mtb* prior to flow cytometric analysis.

RNA sequencing

Lung tissue from WT or MGL-$1^{-/-}$ mice was collected following 8 weeks of *Mtb* infection, preserved in RNA-later, and stored at −80°C prior to RNA isolation. Tissue sections were homogenized and RNA extracted using the RNEASY kit (Qiagen) as instructed by the manufacturer. Five samples per group (WT and MGL-$1^{-/-}$) were submitted to the UTMB Next Generation Sequencing Core Facility. RNA quality was assessed by Aligent Bioanalysis. Following library construction, samples were sequenced on an Illumina NextSeq 550 sequencing system (Illumina). Following mapping to *mus musculus* reference genome, genes were sorted based on adjusted p-value and log2fold change. Statistically significant (adj p-value <0.05) upregulated or downregulated genes were selected for reactome pathway analysis using String database (ELIXIR).

Data availability

RNA Sequencing results are accessible through GEO Series accession number GSE168486 (https://www.ncbi.nlm.nih.gov/geo/query/acc.cgi?acc=GSE168486).

Statistical analysis

Data was analyzed and graphed using GraphPad Prism 8 software and shown as the mean ± SEM. One-way ANOVA followed by a Tukey's test was used for multiple group comparisons. Comparisons between two groups were assessed with a 2-tailed Student's t-test. For all analyses, differences were considered significant at $p<0.05$.

Results

Mtb exposure activates macrophage MGL

To determine if *Mtb* infection activates MGL as part of the host innate response, murine macrophages (RAW 264.7) were infected with *Mtb* H37Rv and expression of MGL-1 and

MGL-2 was assessed by flow cytometry and qPCR. The macrophage mannose receptor (MMR, or CD206) was also measured as a control CLR previously demonstrated to be responsive to *Mtb* infection.

As shown in Fig. 1A, *in vitro* exposure of murine macrophages to *Mtb* led to a marked increase in the surface expression of MGL-1 and a moderate increase in MGL-2. The summarized data in Fig. 1B demonstrates that MGL-1 and 2 were significantly increased beginning at 24 hours post *Mtb* exposure and remained elevated through at least 72 hours. The activation kinetics of MGL-1 in response to *Mtb* exposure were similar to treatment with dexamethasone (1 μM), which has been previously established as a positive control stimuli for human MGL (34). The response kinetics of MGL-1 and MGL-2 were similar following *Mtb* exposure, with a notable difference in the number of macrophages expressing MGL-1 (~10%) compared to MGL-2 (~2%). In contrast to MGL-1, MMR expression was greatest 24 hours post-exposure to *Mtb* and declined at 48 and 72 hours. MGL-2 was poorly responsive to dexamethasone, similar to MMR. To determine if MGL-1 is restricted to the cell surface, or is also present intracellularly, flow cytometry was performed on permeabilized or non-permeablized *Mtb* infected RAW macrophages. As shown in Fig. 1C, *Mtb* exposure led to increased surface expression of MGL. In contrast, there was a limited and non-significant increase in the expression of MGL when cells were stained for both surface and intracellular expression following 24 hours of *Mtb* infection. To assess the presence of total MGL protein, cell lysates were used for western blot analysis (Fig. 1D). Following 24 hours of infection with *Mtb,* MGL protein production by RAW macrophages was found to increase similar to positive control.

To validate the findings of murine cell lines in primary cells, BMDM from C57BL/6 mice were used to detect *mmgl1* and *mmgl2* gene expression following stimulation with *Mtb*. As shown in Fig. 1E, following 24 hours of exposure to *Mtb*, *mmgl1* gene expression was elevated compared to mock. Further assessment of activation kinetics shows that *mmgl1* transcription was detected by 4 hours post *Mtb* and remained elevated until 72 hours (Supplemental Fig. 1A). The homologous gene, *mmgl2,* was increased following 1 hour of *Mtb* infection and was moderately, though non-significantly, elevated from 12–72 hours (Fig. 1E, Supplemental Fig. 1B). These results demonstrated that while RAW macrophages express abundant MGL, primary macrophages appear to regulate the expression of *mmgl* RNA, as well as the turnover of surface expressed MGL translation, more tightly.

Phenotype and localization of MGL$^+$ cells in Mtb-infected lung

To determine if pulmonary cells express MGL in response to *Mtb* infection, a C57BL/6 model of experimental TB was used. Flow cytometric and IHC analysis was performed on lung tissue collected 8 weeks post *Mtb* infection. Analysis of lung tissue by IHC post *Mtb* infection shows localization of MGL expressing cells to sites of inflammation. At varying levels of density in different lesions, MGL$^+$ cell infiltrate was detected adjacent to inflammatory TB lesions (Fig. 2D–F) in C57BL/6 mouse lungs. Interestingly, MGL staining was primarily observed at lesions and less frequently observed in non-inflamed lung parenchyma or interstitium (Fig. 2A, B), similar to the lung of non-infected animals (Fig.

2C). Cells weakly positive for MGL were observed in the lung of non-infected animals (Fig. 2C), suggesting MGL-1^{+} cells may redistribute to sites of *Mtb*-driven inflammation.

Flow cytometric analysis of disrupted lung (Fig. 2G) demonstrates that MGL-1, and not MGL-2, is the predominant receptor expressed in lung of mice infected with *Mtb*. In this flow cytometric analysis, MGL-1expression was primarily observed on cells of the macrophage (F4/80^{+}CD11b^{+}) lineage (Fig. 2G), consistent with previous reports (23, 31). In contrast, MGL-2+ cells were infrequent and similarly observed among F4/80+ and F4/80- populations (Fig. 2G). These data indicate that MGL-1 is likely to be the predominate receptor expressed in the *Mtb* infected lung macrophages and alveolar subpopulations. As a result of these *in vitro* and *in vivo* studies, our subsequent investigations focused on determining the role of macrophage MGL-1 in protective immunity to *Mtb*.

The phenotype of pulmonary macrophages expressing MGL-1 was additionally assessed following 24 hours of *Mtb* exposure in C57BL/6 mice (Fig. 2 H, I). MGL-1 expression was assessed on alveolar macrophages (AMs) (F4/80+CD11c+CD64+Siglec-F+) and interstitial macrophages (IM) (F4/80+CD11c-CD64+Siglec-F-). Assessment of MMR (CD206) was included as a control CLR known to be expressed by AMs and associated with regulatory macrophage function. Following *Mtb* exposure, MGL-1 expression was observed to be restricted to the AM, as compared to the IM, compartment of the lung. Interestingly, AM that express either MGL-1 or MMR, but not both, were observed following *Mtb* exposure (Fig. 2 I).

Impaired anti-mycobacterial and pro-inflammatory activity by MGL-1-deficient macrophages

BMDMs from WT (MGL-1$^{+/+}$) and MGL-1 deficient (MGL-1$^{-/-}$) mice were used to determine whether loss of MGL-1 affects macrophage innate immune outcomes following *Mtb* exposure. Deficiency in MGL-1 signaling was previously shown to promote pro-inflammatory responses to the extracellular bacteria *Klebsiella pneumonia* (27). Due to the known role of MGL to regulate inflammation, cytokine and chemokine pathways were assessed in supernatants of infected macrophages at 4, 12, 24, and 72 hours post *Mtb* infection. Compared to WT, MGL-1$^{-/-}$ macrophages exhibited increased production of proinflammatory cytokines such as IL-1β, IL-6 and TNF-α and chemokines such as RANTES, MIP1β, and MCP-1(Fig. 3A) beginning 12 hours through 72 hours post-*Mtb*. Other anti-inflammatory and T-cell cytokines, such as IL-4, IL-10, IL-13, IFN-γ and IL-2, were either present in low concentrations and/or were not differentially regulated (Fig. 3A). These differential cytokine patterns were independent of effects of MGL-1 deficiency on polarization to M1 or M2 phenotypes in response to *Mtb* infection. As shown in Supplemental Fig. 1C, exposure of BMDMs to *Mtb* promoted an expected increase in M1 (F4/80+CD11b+inos+CD80+) compared to M2 (F4/80+CD11b+arginase+CD206+IL-10+) bias among cells in both WT and MGL-1$^{-/-}$ groups.

A significant increase in mycobacterial growth was also observed in MGL-1$^{-/-}$ macrophages, compared to WT, following 24 hours of infection (Fig. 3B). This was a surprising result in that an antibacterial role for a single CLR pathway is limited in the setting of *Mtb* immunity, and MGL has previously not been associated with regulation of

antimicrobial activity. Further, the inflammatory responses were observed to be elevated 12 hours post-*Mtb,* prior to observed differences in mycobacterial growth (Fig. 3B). Other CLRs mediate phagocytosis of mycobacteria by macrophages, and MGL has been shown to function as an endocytic receptor for other pathogens (e.g. Ebola virus) (35). To determine if the increased bacterial load was influenced by MGL-1-dependent differences in phagocytic uptake, BMDMs were infected with CFSE-labeled *Mtb* followed by flow cytometric assessment. MGL-1-deficient cells were able to internalize *Mtb* similar to WT (Fig. 3C), suggesting the effects on antimicrobial activity are independent from an entry receptor role.

An essential mechanism of host defense against *Mtb* is the production of NO that inhibits mycobacterial growth through nitrositive stress and immune regulation (36, 37). Assessment of nitrite (oxidized form of NO) in cell culture supernatants from 12– 24 hours post-*Mtb* infection demonstrated non-significant changes in NO (Fig. 3D) due to loss of MGL-1 signaling. These results suggest that MGL-1 does not directly regulate mechanisms of bacterial uptake or NO production in the setting of *Mtb* as a mechanism of antimicrobial activity. Additionally, these results indicate that inflammatory dysfunction associated with loss of MGL-1 precedes the defect in antimycobacterial activity.

Pulmonary Mtb proliferation in MGL-1-deficient mice

WT (MGL-$1^{+/+}$) and MGL-$1^{-/-}$ littermates were infected with *Mtb* to determine the *in vivo* role of MGL-1 during pulmonary tuberculosis. Assessment of lung tissue revealed that loss of MGL-1 signaling did not impact pulmonary *Mtb* growth during the early stages of disease (2–4 weeks). However, MGL-1 deficient mice displayed significantly increased pulmonary bacterial burden at 6 and 8 weeks post *Mtb* infection, compared to WT (Fig. 4 A–B).

Lung sections from infected mice were analyzed for histopathological organization of TB lesions in an MGL-1-deficient environment. Representative H&E images from WT and MGL-$1^{-/-}$ mice (Fig. 4C) demonstrate no significant alterations in lung lesion formation, with all groups exhibiting granulomatous inflammation and progressive loss of airspace beginning 4 weeks post infection (Supplemental Fig. 4A, C). MGL+ cells were detectable by IHC staining within inflammatory TB lesions in lung sections from MGL-$1^{-/-}$ mice (Supplemental Fig. 1D), although numbers of positive markings were markedly diminished compared to lung of WT counterparts. These results are consistent with flow cytometric results (Fig. 2G) and represent the presence of small numbers of MGL-2+ cells that are detected with the cross-reactive antibody. Organized lesions were characterized by a majority histiocytic composition in both WT and MGL-$1^{-/-}$ groups at 4, 6, and 8 weeks (Supplemental Fig. 4B). The localization of infiltrating lymphocytes indicated no significant difference in coalescence or organization to bronchial structures (Supplemental Fig. 4E, F). However, there was an increase in lymphocytes associated with lung vessels in the MGL-1-deficient lung following 8 weeks of *Mtb* infection (Supplemental Fig. 4D). Taken together, these results suggest that the increased bacterial burden seen during MGL deficiency is not likely due to significant alterations in development or maintenance of inflammatory lesions harboring the bacilli.

MGL-1 deficiency and exacerbated pulmonary inflammation

Lung homogenate from WT and MGL-$1^{-/-}$ mice was analyzed for differential regulation of cytokine and chemokine secretion. An independent group of MGL-$1^{-/-}$ mice used for this analysis had similar weight gain (Fig. 5A) but also displayed increased lung bacterial burden (Fig. 5B), compared to WT mice. Similar to *in vitro* results observed with BMDMs, multiplex cytokine analysis of lung supernatants revealed a significant pro-inflammatory cytokine signature in the absence of MGL-1. Lung cytokine levels of IL-1β, IL-6, TNF-α, IFN-γ, and IL-12 p40 were significantly increased in MGL-$1^{-/-}$ compared to WT mice (Fig. 5C). A concurrent, significant, increase in IL-10 was also seen in MGL-$1^{-/-}$ lungs, consistent with immune system efforts to dampen excessive inflammatory cytokines. Other cytokines with roles in lymphocyte homeostasis, effector function, and differentiation such as IL-9, IL-2 and IL-17 were not altered due to MGL-1 deficiency. Chemokine levels were also differentially regulated, including significant increases in MCP-1 (Fig. 5), MIP-1-α, and KC (Supplemental Fig. 3I) while levels of other chemokines (e.g. MIP-1β, Eotaxin or RANTES) were similar to WT. These findings expand upon and corroborate the *in vitro* results, suggesting that MGL-1 may regulate the cytokine and chemokine production by pulmonary macrophages following *Mtb* infection

To determine if MGL-1 impairment alters lung-infiltrating populations during TB, total lung leukocytes were isolated from non-infected, and infected, WT or MGL-$1^{-/-}$ mice. Leukocytes were further analyzed based on myeloid and lymphocyte markers (Supplemental Fig. 3A). In both WT and MGL-$1^{-/-}$ infected groups, $CD3^+$, $CD4^+$, and $CD8^+$ T cells were significantly increased due to 8 weeks *Mtb* infection (Supplemental Fig. 3F–H). However, myeloid subset populations displayed no significant difference between WT and MGL-$1^{-/-}$ infected groups (Supplemental Fig 3B–E). These results are consistent with histopathological observations and suggest that deficiency of MGL-1 does not significantly alter cellular influx in murine pulmonary TB.

Accumulation of lipid rich cells in vivo as a result of MGL deficiency

An interesting observation made during histopathological assessment of lung tissue was that of an increased lipid accumulation at sites of *Mtb*-driven inflammation due to MGL deficiency. In lungs harvested at eight weeks post *Mtb* infection, an increased accumulation of foamy macrophage-like cells was observed in TB lesions of MGL-$1^{-/-}$ (Fig. 6B), compared to WT (Fig. 6A), mice. The generation of foamy macrophages is an important feature of TB pathology, serving as a reservoir for latent *Mtb* (38). CLRs have been shown to regulate lipid generation of macrophages through nuclear receptor signaling (39). To further assess the role of MGL-1 in foamy macrophage generation and lipid accumulation, lung leukocytes isolated from infected mice were stained with Nile red and fluorescence was measured by flow cytometry. In the setting of MGL-1 deficiency, the lungs of *Mtb*-infected mice displayed a significant accumulation of nonpolar lipid-rich cells compared to WT counterparts at 8 weeks p.i. (Fig. 6D). At earlier time points, 2 weeks p.i., there was no significant difference in accumulation of Nile red positive cells (Fig. 6C). The results suggest that MGL-1 may contribute to lipid metabolism outcomes of macrophages in the setting of *Mtb* infection.

Differential gene expression due to MGL-1 deficiency

Lung tissue RNA from WT and MGL-$1^{-/-}$ mice infected with *Mtb* for 8 weeks was used to assess differential gene expression by high throughput RNA sequencing. Genome mapping identified 684 significantly (adj p-value <0.05) up-regulated genes and 302 significantly down-regulated genes in the MGL-$1^{-/-}$ compared to WT (Fig. 7A) groups. Included among the up-regulated genes associated with MGL-$1^{-/-}$ (Fig. 7B, C) were genes with described roles in: regulation of cytokine signaling, TLR recognition and signaling cascades, regulation of lipid metabolism, and neutrophil degranulation. Selected genes from the top 12 reactome pathways were validated using qPCR analysis. These genes including, *map3k6, creb5, tlr15, chd9, mmp9,* and *cxcr2* were also determined to be up-regulated based on q-PCR validation in the MGL-$1^{-/-}$ infected group compared to WT (Fig. 7D). Down-regulated genes associated with MGL-$1^{-/-}$ are involved in cellular response to stress, signaling by WNT, and metabolism of amino acids (Supplemental Fig. 2A, B). Individual genes identified among the most downregulated included *fos, krt17, asgr1*, and HSP70 family members *hspa1a and hspa1b*. These results are consistent with changes in lipid accumulation and inflammatory cytokines in the MGL-$1^{-/-}$ lung following *Mtb* infection. The findings further identify candidate molecular pathways whereby MGL-1 may regulate pattern recognition or lipid metabolism responses to *Mtb* and other pathogens that promote pro-inflammatory outcomes and perturb anti-microbial macrophage function.

Discussion

The innate immune response to *Mtb* infection is an important determinant of TB disease progression and outcome. Recognition of mycobacterial antigens by PRRs displayed on the surface of macrophages, a primary host cell for *Mtb*, is especially important for immune activation and clearance of infection (3). Signaling through macrophage PRRs, including TLRs, NLRs, and CLRs, leads to cytokine activation, anti-microbial activity, and differentiation of lymphocyte subsets (8, 19). Identifying and characterizing the diverse PRRs involved in regulating anti-*Mtb* immunity, therefore, is important for efforts to combat TB. Our work makes an important contribution to the understanding of innate immunity to *Mtb* by identifying a new PRR pathway that regulates the host macrophage response to infection. These results are the first demonstration, to our knowledge, that the MGL pathway plays an important immune regulatory and antibacterial role in the innate response of macrophages to mycobacteria.

CLRs are especially abundant on innate myeloid leukocytes and bind carbohydrate motifs of bacterial, viral, and fungal pathogens (40). Similar to other CLRs, we observed that MGL is predominantly expressed by myeloid cells, including post *Mtb* infection. In the lung, alveolar macrophages were observed as the primary population expressing MGL following infection with *Mtb*. Mice express two homologues, MGL-1 and 2, while humans express a single MGL receptor (31). Both MGL-1 and 2 are expressed by murine APCs, however, MGL-1 has been shown to contribute to infectious and inflammatory disease outcomes (27, 41, 42). Consistent with these findings, we observed an upregulation of MGL-1, but not MGL-2, on murine macrophages in response to *Mtb*. In line with other reports, MGL-1 was observed to be expressed predominantly on the cell surface as compared to the intracellular

compartment (43). The MGL^+ cells associated with areas of TB inflammation in lung tissue of infected mice were also presumably MGL-1^+ given the significant reduction of positive MGL markings visualized with IHC and a cross reactive antibody in lung of MGL-1-deficient mice. These data indicate that MGL-1 likely plays a more important role in *Mtb* immunity than its homologue MGL-2. Expanded investigations in MGL-2-deficient and MGL-1/2 double knockout mice will be required to demonstrate a definitive role for MGL-2 in antimycobacterial immunity.

The pathogen-specific moieties of *Mtb* that bind MGL remain to be identified. Specific ligands which are recognized by murine MGL-1 have not been described for any pathogen, to our knowledge. A human chimeric MGL construct was previously shown to bind *E. coli* LPS, and *C. jejuni* lipopolysaccharides and glycoproteins (44, 45). Binding of human MGL to cellular surface receptors (MET, PTK7, SORL1, PTPRF) and integrins (ITGB1, ITGA3) on colorectal cancer cell lines is also described (46). MGL could potentially be activated through recognition of cellular ligands upregulated by *Mtb* infection, an outcome that would be consistent with a defined role for MGL in clearance of apoptotic cells (47). As seen with other CLRs such as Mincle and MMR, mycobacterial cell wall components including lipoarabinomannan and mannosylated proteins may bind MGL and activate macrophage function (10, 11, 15). MGL may also directly bind *Mtb* through galactose or other residues on the mycobacterial membrane that do not bind other CLRs. Identifying the *Mtb* and other pathogen motifs that bind and activate MGL-1 are important to understanding how the CLR repertoire recognizes and integrates diverse danger signals following infections.

Regardless of the mechanism(s) whereby MGL recognizes *Mtb*, our results clearly demonstrate a role for MGL-1 to modulate the pro-inflammatory response. Results from our *in vitro* and *ex vivo* experiments further suggest that these MGL-1-dependent effects on the innate response are mediated primarily by macrophages, although dendritic cells may also contribute. The markedly increased inflammatory response in the lung of mice infected with *Mtb* is also consistent with outcomes observed following *Klebsiella pneumonia* and *T. cruzi* infection (27, 41). Localization of MGL^+ cells to sites of *Mtb* proliferation in the lung further indicate an immune regulatory role. These findings identify MGL-1 among the repertoire of *Mtb*-responsive CLRs that are increasingly understood to be innate immune determinants of cytokine and chemokine outcomes. Among these, pro-inflammatory roles for Mincle, MMR, and the mannose binding CLR DC-SIGN, are well described (15–17, 48). DCIR, Dectin 1, and Dectin 2 also promote pro-inflammatory outcomes to *Mtb* as well, including production of cytokines that regulate Th17 differentiation such as IL-17, IL-6, and TNF-α (14, 49). Our observation that MGL-1 and MMR were expressed by different AM populations may provide an important clue regarding how these various CLRs integrate diverse danger signals and “fine tune” the resulting immune response.

The molecular mechanisms that determine innate immune functions downstream of MGL signaling are poorly described. Ligation of human MGL with glycan agonists activates IL-10 through an NFκB-dependent mechanism that involves ERK and CREB phosphorylation events (50). Interestingly, TNF-α activation downstream of MGL ligation in that system appeared to be NFκB- independent (50). Recently, murine MGL-1-dependent inflammation due to *T. cruzi* infection was associated with differential signaling through ERK1,2 and NF-

κB (41). These are also important transcription factors for several inflammatory outcomes in the context of *Mtb* (51) that are driven by multiple PRR systems. To begin to understand MGL-1 dependent activation by *Mtb*, we conducted a differential transcriptome analysis of lung RNA from infected WT and MGL-$1^{-/-}$ mice. The differential analysis supports and expands our observations that MGL-1 regulates pro-inflammatory responses. In the absence of MGL-1, *Mtb* infection of the lung led to significantly increased activation of multiple immune recognition and immune response networks, including TLR pathways (TLR7, 8, and 13). Recognition of *Mtb* by TLRs plays an important role in regulation of downstream immune responses and activation of pro-inflammatory cytokines (9). Significant up-regulation of TLR8, for example, is seen in TB patients during the acute phase of disease and has been linked to TB susceptibility in men (52).

Included among several differentially activated genes that were upregulated due to MGL-1 loss were *nfκb, map3k6*, and *creb5*, which have roles in activation of broad inflammation networks, and precision inflammation outcomes, respectively. We additionally observed increased *stat3* in the MGL-$1^{-/-}$ group, which has been shown to regulate several cytokine pathways, including IL-10, and diminish T cell mediated control of *Mtb* infection and growth (53). MGL-1 deficiency was also associated with decreased expression of several other genes. Among the top 12 downregulated genes were the Hsp70 family members *hspa1a* and *hspa1b*. These proteins serve as molecular chaperones to maintain protein quality control and reduce inflammation by regulating protein folding and degradation pathways (54, 55). Another gene that is downregulated in the absence of MGL-1 is *fos*. The FOS family members form heterodimers with JUN family members as part of the AP-1 transcription factor complex and are implicated in cellular differentiation and apoptosis as well as phospholipid synthesis (56). An unexpected downregulation due to MGL-1 deficiency was *krt17*, which encodes Keratin 17 (K17). In skin keratinocytes, K17 was shown to interact with the TNFR-1 associated death domain protein (TRADD), and K17-deficient mice displayed increased NF-κB activation (57). Further exploration of these candidate mechanisms is needed to determine MGL-1-dependent roles in regulation of inflammatory or other immune outcomes following *Mtb* infection.

It is also possible that MGL-1 signaling enhances or modifies activation through other PRR (58). Co-signaling of MGL with TLR2, in preference to other TLRs, was previously shown as a mechanism of molecular synergy that alters post-activation cytokine outcomes (50). TLR2 is also important for innate immune activation of macrophages by *Mtb* and has been shown to bind several mycobacterial lipoproteins and lipoglycans (59). We also observed that MGL-1 deficiency leads to downregulation of the related gene *asgr1*, which encodes the Asialoglycoprotein Receptor 1 (ASGR1, CLEC4H1). Like MGL-1, ASGR1 binds to serum proteins with exposed galactose or N-acetyl-galactosamine residues and targets them to the lysosome for degradation (60). Further investigation is needed to determine whether ASGR1 or other pattern recognition systems are differentially regulated by MGL-1 and the potential impact on immune outcomes. These individual, complementary, or convergent signaling mechanisms may be important mechanisms whereby MGL-1 and other CLRs generate specificity in effector function or limit excessive inflammation following infections.

Importantly, our work also identifies an MGL-1-dependent role in the antimycobacterial function of macrophages. Both BMDMs and lungs of MGL-1$^{-/-}$ mice supported greater mycobacterial burden. These results contrast those of a previous report in a murine model of bacterial pneumonia. In that model, MGL-1-deficient mice infected with *Klebsiella pneumonia* displayed inflammatory pathology in the absence of changes in bacterial burden (27). The results are exciting, as evidence for *in vivo* antimycobacterial roles for CLRs is limited. The Clecsf8 molecule expressed by neutrophils and monocytes has been shown to modulate the pulmonary burden of *Mtb*-infected mice (61). Additionally, impairment of DC-SIGN is associated with reduced mycobacterial growth within macrophages *in vitro* (16). However, only mice deficient in SIGNR3, a homologue of DC-SIGN, displayed increased mycobacterial growth in their lungs compared to WT (62).

The innate immune basis for MGL-1 antimycobacterial macrophage activity remains to be identified. Regulation of phagocytic activity and NO in innate responses to *Mtb* have been described for MMR and Mincle, respectively (15, 17), however, these responses were not sufficient to impact mycobacterial burden *in vivo*. In contrast to these outcomes previously described for Mincle and MMR, loss of MGL-1 in our studies did not affect the production of NO nor phagocytic uptake by murine macrophages following *Mtb* infection. This outcome also differs from recent observations of *T. cruzi* infection, where MGL-1 deficiency promoted significant increases in NO production by macrophages (41). Potentially, inflammatory outcomes could indirectly contribute to bacterial proliferation as described (63–65) and previously suggested as a basis for the *in vitro* effects of DC-SIGN impairment (16). Following *Klebsiella pneumonia* infection, a marked influx of neutrophils and activation of neutrophil mediators (MMP9 and MPO) was described in MGL-1$^{-/-}$ mice compared to WT (27). We did not observe significant changes in neutrophil influx due to MGL-1 deficiency in mice with pulmonary TB. However, our differential transcriptome analysis revealed significant increases in genes that regulate neutrophil activation including *mmp9*, as well as *s100a9* and *cxcr2*. These findings support further investigations to determine if loss of MGL signaling could contribute to defects in neutrophil function that are important for immunity to *Mtb*. These effects would likely be indirect since MGL expression is primarily restricted to macrophages and DCs.

The MGL-1-dependent effects on macrophage lipid metabolism that we observed following *Mtb* infection also has important implications. Sequestration of host lipids serves as an important pathogenesis mechanism used by *Mtb* and provides for a primary nutrient resource for growth and persistence in macrophages (66). Our results demonstrate a significant accumulation of host lipids in pulmonary macrophages of MGL-1-deficient mice infected with *Mtb,* suggesting that MGL-1 may regulate lipid metabolism processes activated by infection. Other CLRs, such as MMR and Dectin 1, have been shown to regulate inflammatory lipids (67). Recognition of *Mtb* by MMR induces peroxisome proliferator-activated receptor (PPAR)-γ, a nuclear receptor which regulates lipid metabolism and inflammatory cytokine responses (67). Differentiation and anti-inflammatory function of alternatively activated macrophages is also regulated by PPAR-γ (68). Both MGL and MMR are markers of alternative macrophage activation, however, we observed a mutually exclusive pattern of expression by AM following pulmonary *Mtb* infection. Differential transcriptome analysis in our study revealed an

upregulation of *ppar*-α and several genes in a lipid metabolism pathway regulated by PPAR-α such as the transcriptional co-activator and epigenetic modifier *chd9*. This is an interesting observation since PPAR-α is a member of the PPAR superfamily along with PPAR-γ (69) and is a major regulator of lipid metabolism as well as inflammation (70). These results provide important direction for the mechanisms whereby MGL-1 signaling may regulate lipid metabolism, potentially including inflammatory lipids that have been associated with TB pathogenesis (71). Long term, analysis of the differential profile of lipids in lungs of MGL-1 deficient mice may offer clues that help identify the regulatory networks for MGL-1 signaling and further suggest mechanisms for the increased inflammation and bacterial growth.

In conclusion, we have demonstrated an immunomodulatory and anti-bacterial role for the murine MGL-1 receptor during *Mtb* infection *in vitro* and *in vivo.* These results suggest that MGL-1 has a unique function compared to many CLR pathways which promote pro-inflammatory processes associated with TB pathogenesis. Further studies are needed to define how MGL-1 is regulated in the context of *Mtb* infection and identify the mechanistic role in lipid accumulation. Nonetheless, these results identify MGL-1 as an important host receptor in immunity to *Mtb* with potential for exploitation in host directed therapies intended to reduce inflammatory pathology or limit bacterial proliferation.

Supplementary Material

Refer to Web version on PubMed Central for supplementary material.

Acknowledgments

The authors would like to extend our gratitude to Maki Wakamiya from UTMB's transgenic mouse core for her help with breeding and husbandry of mouse colonies. We would additionally like to thank Mark Griffin and Dr. Yuejin Liang from UTMB's flow cytometry core for their guidance with all flow cytometry experiments. The authors thank Dr. Steve Widen from UTMB's Next Generation Sequencing core for assistance with RNA sequencing experimentation and James Fisher for assistance with sequencing analysis. Finally, the authors thank the Animal Resource Care team at UTMB for all experimental animal husbandry and care.

Funding: This work was supported by National Institutes of Health (NIH), National Institute of Allergy and Infectious Diseases (NIAID) grant R61AI138328 (to B.B.G and J.J.E) and by the University of Texas Medical Branch James W. McLaughlin Endowment Pre-doctoral Fellowship (to K.F.N.).

References

1. World Health Organization. Global Tuberculosis Report 2019. Geneva, Switzerland: WHO, Programme GT; 2019 CC BY-NC-SA 3.0 IGO.
2. Partnership ST 2020. The Potential Impact of the COVID-19 Response on Tuberculosis in High-Burden Countries: a Modeling Analysis.
3. Kleinnijenhuis J, Oosting M, Joosten LA, Netea MG, and Van Crevel R. 2011. Innate immune recognition of Mycobacterium tuberculosis. Clin Dev Immunol 2011: 405310. [PubMed: 21603213]
4. Shi J, Sun BH, Zhou LR, and Wang XS. 2016. Role of IL-10 and TNF-alpha during *Mycobacterium tuberculosis* infection in murine alveolar macrophages. Genet Mol Res 15.
5. Cohen SB, Gern BH, Delahaye JL, Adams KN, Plumlee CR, Winkler JK, Sherman DR, Gerner MY, and Urdahl KB. 2018. Alveolar Macrophages Provide an Early *Mycobacterium tuberculosis* Niche and Initiate Dissemination. Cell Host Microbe 24: 439–446 e434. [PubMed: 30146391]
6. Khan A, Singh VK, Hunter RL, and Jagannath C. 2019. Macrophage heterogeneity and plasticity in tuberculosis. J Leukoc Biol 106: 275–282. [PubMed: 30938876]

7. Kahnert A, Seiler P, Stein M, Bandermann S, Hahnke K, Mollenkopf H, and Kaufmann SH. 2006. Alternative activation deprives macrophages of a coordinated defense program to *Mycobacterium tuberculosis*. Eur J Immunol 36: 631–647. [PubMed: 16479545]
8. Mortaz E, Adcock IM, Tabarsi P, Masjedi MR, Mansouri D, Velayati AA, Casanova JL, and Barnes PJ. 2015. Interaction of Pattern Recognition Receptors with *Mycobacterium Tuberculosis*. J Clin Immunol 35: 1–10.
9. Liu CH, Liu H, and Ge B. 2017. Innate immunity in tuberculosis: host defense vs pathogen evasion. Cell Mol Immunol 14: 963–975. [PubMed: 28890547]
10. Torrelles JB, and Schlesinger LS. 2010. Diversity in *Mycobacterium tuberculosis* mannosylated cell wall determinants impacts adaptation to the host. Tuberculosis (Edinb) 90: 84–93. [PubMed: 20199890]
11. Kang PB, Azad AK, Torrelles JB, Kaufman TM, Beharka A, Tibesar E, DesJardin LE, and Schlesinger LS. 2005. The human macrophage mannose receptor directs *Mycobacterium tuberculosis* lipoarabinomannan-mediated phagosome biogenesis. J Exp Med 202: 987–999. [PubMed: 16203868]
12. Velasquez LN, Stuve P, Gentilini MV, Swallow M, Bartel J, Lycke NY, Barkan D, Martina M, Lujan HD, Kalay H, van Kooyk Y, Sparwasser TD, and Berod L. 2018. Targeting *Mycobacterium tuberculosis* Antigens to Dendritic Cells via the DC-Specific-ICAM3-Grabbing-Nonintegrin Receptor Induces Strong T-Helper 1 Immune Responses. Front Immunol 9: 471. [PubMed: 29662482]
13. Yonekawa A, Saijo S, Hoshino Y, Miyake Y, Ishikawa E, Suzukawa M, Inoue H, Tanaka M, Yoneyama M, Oh-Hora M, Akashi K, and Yamasaki S. 2014. Dectin-2 is a direct receptor for mannose-capped lipoarabinomannan of mycobacteria. Immunity 41: 402–413. [PubMed: 25176311]
14. van de Veerdonk FL, Teirlinck AC, Kleinnijenhuis J, Kullberg BJ, van Crevel R, van der Meer JW, Joosten LA, and Netea MG. 2010. *Mycobacterium tuberculosis* induces IL-17A responses through TLR4 and dectin-1 and is critically dependent on endogenous IL-1. J Leukoc Biol 88: 227–232. [PubMed: 20299682]
15. Lang R 2013. Recognition of the mycobacterial cord factor by Mincle: relevance for granuloma formation and resistance to tuberculosis. Front Immunol 4: 5. [PubMed: 23355839]
16. Lugo-Villarino G, Troegeler A, Balboa L, Lastrucci C, Duval C, Mercier I, Benard A, Capilla F, Al Saati T, Poincloux R, Kondova I, Verreck FAW, Cougoule C, Maridonneau-Parini I, Sasiain MDC, and Neyrolles O. 2018. The C-Type Lectin Receptor DC-SIGN Has an Anti-Inflammatory Role in Human M(IL-4) Macrophages in Response to *Mycobacterium tuberculosis*. Front Immunol 9: 1123. [PubMed: 29946317]
17. Rajaram MVS, Arnett E, Azad AK, Guirado E, Ni B, Gerberick AD, He LZ, Keler T, Thomas LJ, Lafuse WP, and Schlesinger LS. 2017. *M. tuberculosis*-Initiated Human Mannose Receptor Signaling Regulates Macrophage Recognition and Vesicle Trafficking by FcRgamma-Chain, Grb2, and SHP-1. Cell Rep 21: 126–140. [PubMed: 28978467]
18. Heitmann L, Schoenen H, Ehlers S, Lang R, and Holscher C. 2013. Mincle is not essential for controlling *Mycobacterium tuberculosis* infection. Immunobiology 218: 506–516. [PubMed: 22784441]
19. Mishra A, Akhtar S, Jagannath C, and Khan A. 2017. Pattern recognition receptors and coordinated cellular pathways involved in tuberculosis immunopathogenesis: Emerging concepts and perspectives. Mol Immunol 87: 240–248. [PubMed: 28514713]
20. Marakalala MJ, Guler R, Matika L, Murray G, Jacobs M, Brombacher F, Rothfuchs AG, Sher A, and Brown GD. 2011. The Syk/CARD9-coupled receptor Dectin-1 is not required for host resistance to *Mycobacterium tuberculosis* in mice. Microbes Infect 13: 198–201. [PubMed: 21034845]
21. Geijtenbeek TB, and Gringhuis SI. 2009. Signalling through C-type lectin receptors: shaping immune responses. Nat Rev Immunol 9: 465–479. [PubMed: 19521399]
22. Zizzari IG, Napoletano C, Battisti F, Rahimi H, Caponnetto S, Pierelli L, Nuti M, and Rughetti A. 2015. MGL Receptor and Immunity: When the Ligand Can Make the Difference. J Immunol Res 2015: 450695. [PubMed: 26839900]

23. Kaori Denda-Nagai TI 2016. MGL/CD301 as a Unique C-Type Lectin Expressed on Dendritic Cells and Macrophages. In C-Type Lectin Receptors in Immunity. Springer, Tokyo. 165–178.
24. Napoletano C, Rughetti A, Agervig Tarp MP, Coleman J, Bennett EP, Picco G, Sale P, Denda-Nagai K, Irimura T, Mandel U, Clausen H, Frati L, Taylor-Papadimitriou J, Burchell J, and Nuti M. 2007. Tumor-associated Tn-MUC1 glycoform is internalized through the macrophage galactose-type C-type lectin and delivered to the HLA class I and II compartments in dendritic cells. Cancer Res 67: 8358–8367. [PubMed: 17804752]
25. Dusoswa SA, Verhoeff J, Abels E, Mendez-Huergo SP, Croci DO, Kuijper LH, de Miguel E, Wouters V, Best MG, Rodriguez E, Cornelissen LAM, van Vliet SJ, Wesseling P, Breakefield XO, Noske DP, Wurdinger T, Broekman MLD, Rabinovich GA, van Kooyk Y, and Garcia-Vallejo JJ. 2020. Glioblastomas exploit truncated O-linked glycans for local and distant immune modulation via the macrophage galactose-type lectin. Proc Natl Acad Sci U S A 117: 3693–3703. [PubMed: 32019882]
26. Eggink LL, Roby KF, Cote R, and Kenneth Hoober J. 2018. An innovative immunotherapeutic strategy for ovarian cancer: CLEC10A and glycomimetic peptides. J Immunother Cancer 6: 28. [PubMed: 29665849]
27. Jondle CN, Sharma A, Simonson TJ, Larson B, Mishra BB, and Sharma J. 2016. Macrophage Galactose-Type Lectin-1 Deficiency Is Associated with Increased Neutrophilia and Hyperinflammation in Gram-Negative Pneumonia. J Immunol 196: 3088–3096. [PubMed: 26912318]
28. Vukman KV, Ravida A, Aldridge AM, and O'Neill SM. 2013. Mannose receptor and macrophage galactose-type lectin are involved in *Bordetella pertussis* mast cell interaction. J Leukoc Biol 94: 439–448. [PubMed: 23794711]
29. van Vliet SJ, Steeghs L, Bruijns SC, Vaezirad MM, Snijders Blok C, Arenas Busto JA, Deken M, van Putten JP, and van Kooyk Y. 2009. Variation of *Neisseria gonorrhoeae* lipooligosaccharide directs dendritic cell-induced T helper responses. PLoS Pathog 5: e1000625. [PubMed: 19834553]
30. Huante MB, Saito TB, Nusbaum RJ, Naqvi KF, Chauhan S, Hunter RL, Actor JK, Rudra JS, Endsley MA, Lisinicchia JG, Gelman BB, and Endsley JJ. 2020. Small Animal Model of Post-chemotherapy Tuberculosis Relapse in the Setting of HIV Co-infection. Front Cell Infect Microbiol 10: 150. [PubMed: 32373548]
31. Singh SK, Streng-Ouwehand I, Litjens M, Weelij DR, Garcia-Vallejo JJ, van Vliet SJ, Saeland E, and van Kooyk Y. 2009. Characterization of murine MGL1 and MGL2 C-type lectins: distinct glycan specificities and tumor binding properties. Mol Immunol 46: 1240–1249. [PubMed: 19162326]
32. Nusbaum RJ, Calderon VE, Huante MB, Sutjita P, Vijayakumar S, Lancaster KL, Hunter RL, Actor JK, Cirillo JD, Aronson J, Gelman BB, Lisinicchia JG, Valbuena G, and Endsley JJ. 2016. Pulmonary Tuberculosis in Humanized Mice Infected with HIV-1. Sci Rep 6: 21522. [PubMed: 26908312]
33. Massey S, Yeager LA, Blumentritt CA, Vijayakumar S, Sbrana E, Peterson JW, Brasel T, LeDuc JW, Endsley JJ, and Torres AG. 2014. Comparative *Burkholderia pseudomallei* natural history virulence studies using an aerosol murine model of infection. Sci Rep 4: 4305. [PubMed: 24603493]
34. van Vliet SJ, Gringhuis SI, Geijtenbeek TB, and van Kooyk Y. 2006. Regulation of effector T cells by antigen-presenting cells via interaction of the C-type lectin MGL with CD45. Nat Immunol 7: 1200–1208. [PubMed: 16998493]
35. Takada A, Fujioka K, Tsuiji M, Morikawa A, Higashi N, Ebihara H, Kobasa D, Feldmann H, Irimura T, and Kawaoka Y. 2004. Human macrophage C-type lectin specific for galactose and N-acetylgalactosamine promotes filovirus entry. J Virol 78: 2943–2947. [PubMed: 14990712]
36. Jayakumar D, Jacobs WR Jr., and Narayanan S. 2008. Protein kinase E of *Mycobacterium tuberculosis* has a role in the nitric oxide stress response and apoptosis in a human macrophage model of infection. Cell Microbiol 10: 365–374. [PubMed: 17892498]
37. Mishra BB, Lovewell RR, Olive AJ, Zhang G, Wang W, Eugenin E, Smith CM, Phuah JY, Long JE, Dubuke ML, Palace SG, Goguen JD, Baker RE, Nambi S, Mishra R, Booty MG, Baer CE, Shaffer SA, Dartois V, McCormick BA, Chen X, and Sassetti CM. 2017. Nitric oxide prevents

a pathogen-permissive granulocytic inflammation during tuberculosis. Nat Microbiol 2: 17072. [PubMed: 28504669]

38. Shim D, Kim H, and Shin SJ. 2020. *Mycobacterium tuberculosis* Infection-Driven Foamy Macrophages and Their Implications in Tuberculosis Control as Targets for Host-Directed Therapy. Front Immunol 11: 910. [PubMed: 32477367]
39. Sancho D, and Reis e Sousa C. 2012. Signaling by myeloid C-type lectin receptors in immunity and homeostasis. Annu Rev Immunol 30: 491–529. [PubMed: 22224766]
40. Raymond BBA, Neyrolles O, and Rombouts Y. 2020. C-type Lectins in Immunity to Lung Pathogens. Curr Top Microbiol Immunol.
41. Rodriguez T, Pacheco-Fernandez T, Vazquez-Mendoza A, Nieto-Yanez O, Juarez-Avelar I, Reyes JL, Terrazas LI, and Rodriguez-Sosa M. 2020. MGL1 Receptor Plays a Key Role in the Control of T. cruzi Infection by Increasing Macrophage Activation through Modulation of ERK1/2, c-Jun, NF-kappaB and NLRP3 Pathways. Cells 9.
42. Montero-Barrera D, Valderrama-Carvajal H, Terrazas CA, Rojas-Hernandez S, Ledesma-Soto Y, Vera-Arias L, Carrasco-Yepez M, Gomez-Garcia L, Martinez-Saucedo D, Becerra-Diaz M, and Terrazas LI. 2015. The macrophage galactose-type lectin-1 (MGL1) recognizes *Taenia crassiceps* antigens, triggers intracellular signaling, and is critical for resistance to this infection. Biomed Res Int 2015: 615865. [PubMed: 25664320]
43. Denda-Nagai K, Aida S, Saba K, Suzuki K, Moriyama S, Oo-Puthinan S, Tsuiji M, Morikawa A, Kumamoto Y, Sugiura D, Kudo A, Akimoto Y, Kawakami H, Bovin NV, and Irimura T. 2010. Distribution and function of macrophage galactose-type C-type lectin 2 (MGL2/CD301b): efficient uptake and presentation of glycosylated antigens by dendritic cells. J Biol Chem 285: 19193–19204. [PubMed: 20304916]
44. Maalej M, Forgione RE, Marchetti R, Bulteau F, Thépaut M, Lanzetta R, Laguri C, Simorre J-P, Fieschi F, Molinaro A, and Silipo A. 2019. Human Macrophage Galactose-Type Lectin (MGL) Recognizes the Outer Core of *Escherichia coli* Lipooligosaccharide. ChemBioChem 20: 1778–1782. [PubMed: 30919527]
45. van Sorge NM, Bleumink NM, van Vliet SJ, Saeland E, van der Pol WL, van Kooyk Y, and van Putten JP. 2009. N-glycosylated proteins and distinct lipooligosaccharide glycoforms of *Campylobacter jejuni* target the human C-type lectin receptor MGL. Cell Microbiol 11: 1768–1781. [PubMed: 19681908]
46. Pirro M, Rombouts Y, Stella A, Neyrolles O, Burlet-Schiltz O, van Vliet SJ, de Ru AH, Mohammed Y, Wuhrer M, van Veelen PA, and Hensbergen PJ. 2020. Characterization of Macrophage Galactose-type Lectin (MGL) ligands in colorectal cancer cell lines. Biochim Biophys Acta Gen Subj 1864: 129513.
47. Yuita H, Tsuiji M, Tajika Y, Matsumoto Y, Hirano K, Suzuki N, and Irimura T. 2005. Retardation of removal of radiation-induced apoptotic cells in developing neural tubes in macrophage galactose-type C-type lectin-1-deficient mouse embryos. Glycobiology 15: 1368–1375. [PubMed: 16096344]
48. Tanne A, and Neyrolles O. 2010. C-type lectins in immune defense against pathogens: the murine DC-SIGN homologue SIGNR3 confers early protection against *Mycobacterium tuberculosis* infection. Virulence 1: 285–290. [PubMed: 21178456]
49. Troegeler A, Mercier I, Cougoule C, Pietretti D, Colom A, Duval C, Vu Manh TP, Capilla F, Poincloux R, Pingris K, Nigou J, Rademann J, Dalod M, Verreck FA, Al Saati T, Lugo-Villarino G, Lepenies B, Hudrisier D, and Neyrolles O. 2017. C-type lectin receptor DCIR modulates immunity to tuberculosis by sustaining type I interferon signaling in dendritic cells. Proc Natl Acad Sci U S A 114: E540–E549. [PubMed: 28069953]
50. van Vliet SJ, Bay S, Vuist IM, Kalay H, Garcia-Vallejo JJ, Leclerc C, and van Kooyk Y. 2013. MGL signaling augments TLR2-mediated responses for enhanced IL-10 and TNF-alpha secretion. J Leukoc Biol 94: 315–323. [PubMed: 23744646]
51. van Kooyk Y, Ilarregui JM, and van Vliet SJ. 2015. Novel insights into the immunomodulatory role of the dendritic cell and macrophage-expressed C-type lectin MGL. Immunobiology 220: 185–192. [PubMed: 25454488]
52. Davila S, Hibberd ML, Hari Dass R, Wong HE, Sahiratmadja E, Bonnard C, Alisjahbana B, Szeszko JS, Balabanova Y, Drobniewski F, van Crevel R, van de Vosse E, Nejentsev S, Ottenhoff

TH, and Seielstad M. 2008. Genetic association and expression studies indicate a role of toll-like receptor 8 in pulmonary tuberculosis. PLoS Genet 4: e1000218. [PubMed: 18927625]

53. Gao Y, Basile JI, Classon C, Gavier-Widen D, Yoshimura A, Carow B, and Rottenberg ME. 2018. STAT3 expression by myeloid cells is detrimental for the T- cell-mediated control of infection with *Mycobacterium tuberculosis*. PLoS Pathog 14: e1006809. [PubMed: 29338039]
54. Fernández-Fernández MR, Gragera M, Ochoa-Ibarrola L, Quintana-Gallardo L, and Valpuesta JM. 2017. Hsp70 - a master regulator in protein degradation. FEBS Lett 591: 2648–2660. [PubMed: 28696498]
55. Henderson B, and Pockley AG. 2010. Molecular chaperones and protein-folding catalysts as intercellular signaling regulators in immunity and inflammation. J Leukoc Biol 88: 445–462. [PubMed: 20445014]
56. Rodríguez-Berdini L, and Caputto BL. 2019. Lipid Metabolism in Neurons: A Brief Story of a Novel c-Fos-Dependent Mechanism for the Regulation of Their Synthesis. Frontiers in Cellular Neuroscience 13. [PubMed: 30766479]
57. Tong X, and Coulombe PA. 2006. Keratin 17 modulates hair follicle cycling in a TNFalpha-dependent fashion. Genes Dev 20: 1353–1364. [PubMed: 16702408]
58. Naqvi KF, and Endsley JJ. 2020. Myeloid C-Type Lectin Receptors in Tuberculosis and HIV Immunity: Insights Into Co-infection? Front Cell Infect Microbiol 10: 263. [PubMed: 32582566]
59. Shukla S, Richardson ET, Drage MG, Boom WH, and Harding CV. 2018. *Mycobacterium tuberculosis* Lipoprotein and Lipoglycan Binding to Toll-Like Receptor 2 Correlates with Agonist Activity and Functional Outcomes. Infect Immun 86.
60. Hoober JK 2020. ASGR1 and Its Enigmatic Relative, CLEC10A. International Journal of Molecular Sciences 21: 4818.
61. Wilson GJ, Marakalala MJ, Hoving JC, van Laarhoven A, Drummond RA, Kerscher B, Keeton R, van de Vosse E, Ottenhoff TH, Plantinga TS, Alisjahbana B, Govender D, Besra GS, Netea MG, Reid DM, Willment JA, Jacobs M, Yamasaki S, van Crevel R, and Brown GD. 2015. The C-type lectin receptor CLECSF8/CLEC4D is a key component of anti-mycobacterial immunity. Cell Host Microbe 17: 252–259. [PubMed: 25674984]
62. Tanne A, Ma B, Boudou F, Tailleux L, Botella H, Badell E, Levillain F, Taylor ME, Drickamer K, Nigou J, Dobos KM, Puzo G, Vestweber D, Wild MK, Marcinko M, Sobieszczuk P, Stewart L, Lebus D, Gicquel B, and Neyrolles O. 2009. A murine DC-SIGN homologue contributes to early host defense against *Mycobacterium tuberculosis*. J Exp Med 206: 2205–2220. [PubMed: 19770268]
63. Hawn TR, Matheson AI, Maley SN, and Vandal O. 2013. Host-directed therapeutics for tuberculosis: can we harness the host? Microbiol Mol Biol Rev 77: 608–627. [PubMed: 24296574]
64. Tobin DM, Roca FJ, Ray JP, Ko DC, and Ramakrishnan L. 2013. An enzyme that inactivates the inflammatory mediator leukotriene b4 restricts mycobacterial infection. PloS one 8: e67828. [PubMed: 23874453]
65. Vilaplana C, Marzo E, Tapia G, Diaz J, Garcia V, and Cardona PJ. 2013. Ibuprofen therapy resulted in significantly decreased tissue bacillary loads and increased survival in a new murine experimental model of active tuberculosis. The Journal of infectious diseases 208: 199–202. [PubMed: 23564636]
66. Lee W, VanderVen BC, Fahey RJ, and Russell DG. 2013. Intracellular *Mycobacterium tuberculosis* exploits host-derived fatty acids to limit metabolic stress. J Biol Chem 288: 6788–6800. [PubMed: 23306194]
67. Rajaram MV, Brooks MN, Morris JD, Torrelles JB, Azad AK, and Schlesinger LS. 2010. *Mycobacterium tuberculosis* activates human macrophage peroxisome proliferator-activated receptor gamma linking mannose receptor recognition to regulation of immune responses. J Immunol 185: 929–942. [PubMed: 20554962]
68. Bouhlel MA, Derudas B, Rigamonti E, Dievart R, Brozek J, Haulon S, Zawadzki C, Jude B, Torpier G, Marx N, Staels B, and Chinetti-Gbaguidi G. 2007. PPARgamma activation primes human monocytes into alternative M2 macrophages with anti-inflammatory properties. Cell Metab 6: 137–143. [PubMed: 17681149]

69. Tyagi S, Gupta P, Saini AS, Kaushal C, and Sharma S. 2011. The peroxisome proliferator-activated receptor: A family of nuclear receptors role in various diseases. J Adv Pharm Technol Res 2: 236–240. [PubMed: 22247890]

70. Bougarne N, Weyers B, Desmet SJ, Deckers J, Ray DW, Staels B, and De Bosscher K. 2018. Molecular Actions of PPARα in Lipid Metabolism and Inflammation. Endocr Rev 39: 760–802. [PubMed: 30020428]

71. Dietzold J, Gopalakrishnan A, and Salgame P. 2015. Duality of lipid mediators in host response against *Mycobacterium tuberculosis*: good cop, bad cop. F1000Prime Rep 7: 29. [PubMed: 25926980]

KEY POINTS

- Macrophage Galactose-type Lectin-1 (MGL-1, or CLEC10A) is activated by *Mtb*
- MGL-1 plays important role in controlling mycobacterial proliferation in lung
- Loss of MGL-1 promotes pro-inflammatory cytokines and lipid accumulation in TB

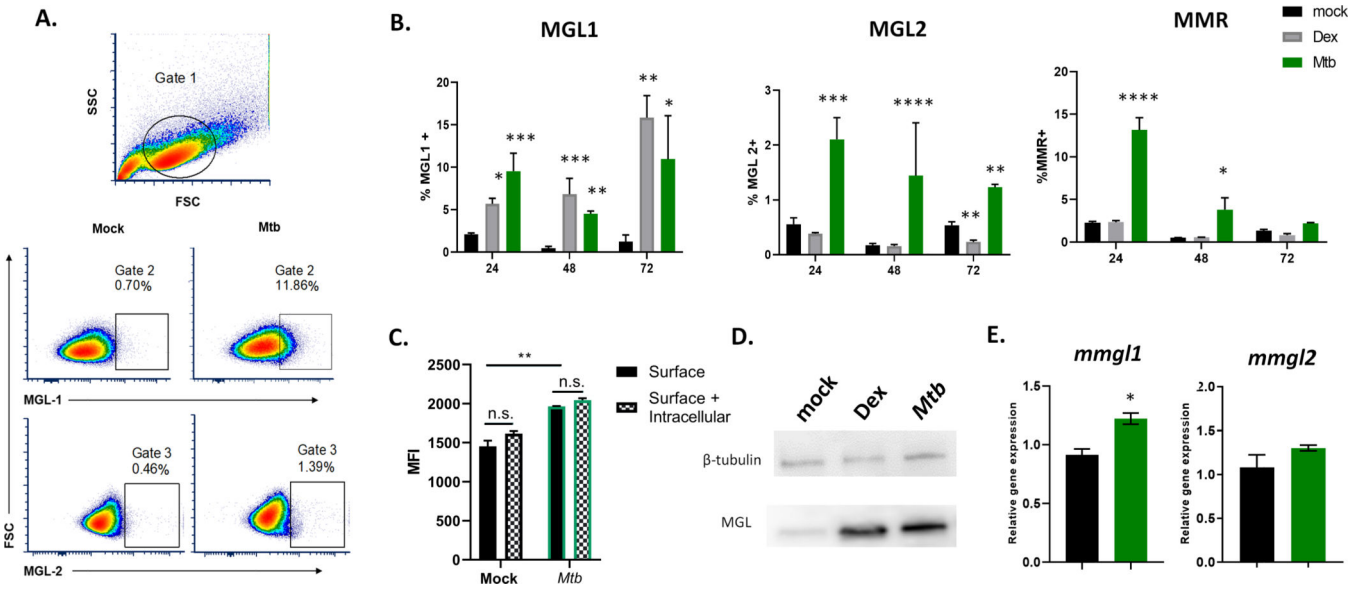

FIGURE 1. *Mtb* exposure activates macrophage MGL.

RAW 264.7 macrophages were stimulated with dexamethasone (1 μM) or 10 MOI of *Mtb* H37Rv for 24, 48, and 72 hours. Changes in surface expression of MGL1, MGL2, and mannose receptor (MMR) were assessed by flow cytometry. (A) Gating strategy for flow cytometric analysis, and (B) summarized flow cytometric data of marker expression by macrophages. (C) Surface and intracellular MGL-1 expression was assessed by flow cytometry analysis of Raw macrophages infected with *Mtb* for 24 hours. (D) Analysis of total cellular MGL by western blot following 24 hours of treatment with mock, dexamethasone, or *Mtb*. (E) Expression of *mmgl1* and *mmgl2* by BMDM following treatment with *Mtb* for 24 hours, as measured by qPCR. Data shown are representative of at least two independent experiments of n=3 per experiment. Statistical analysis was performed by using one-way ANOVA followed by tukey's test for multiple comparisons. Significant differences compared to mock treatment are indicated with ****p<0.0001, ***p<0.001, **p<0.01, and *p<0.05.

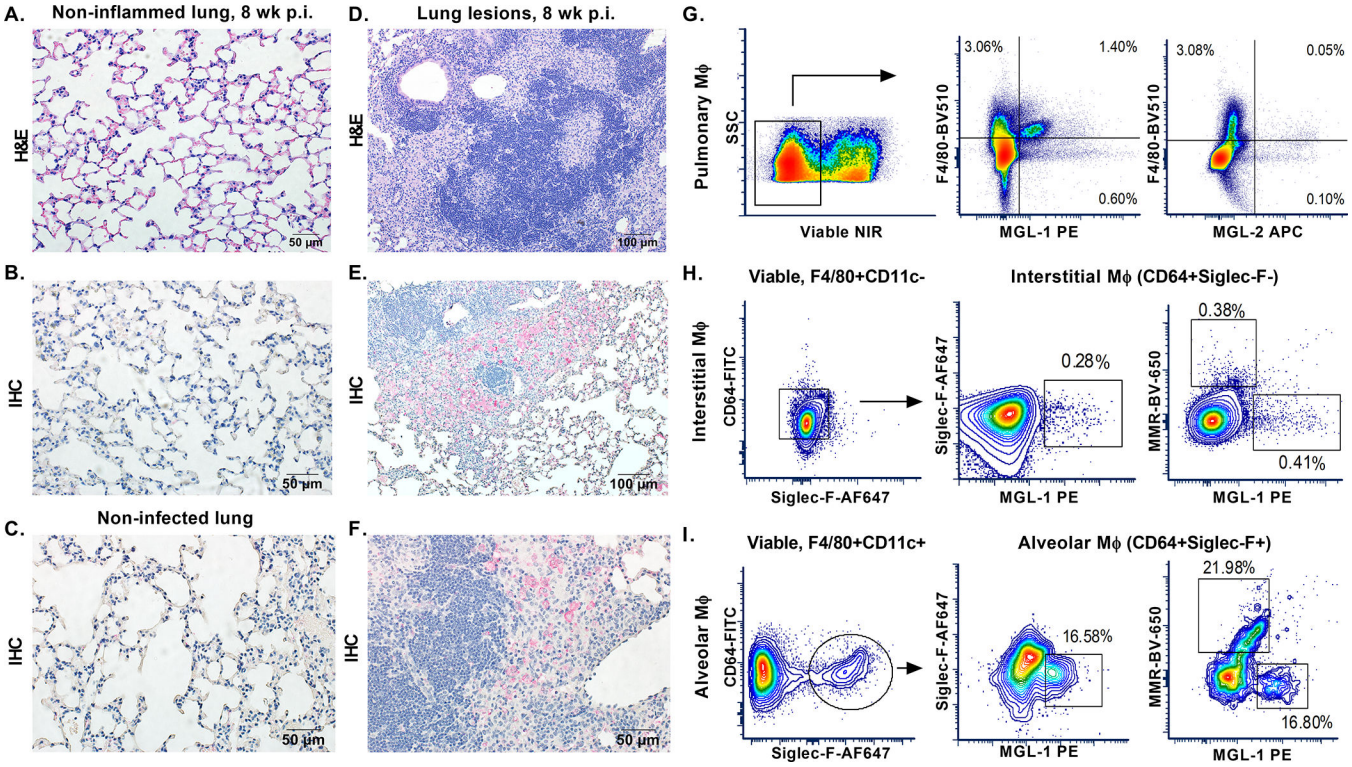

FIGURE 2. MGL-1+ macrophages localize to sites of *Mtb*-driven inflammation in the lung.

WT C57BL/6 mice (n=5) were infected with *Mtb* for 8 weeks or non-infected. Lung sections were used to assess pulmonary histopathology using H&E, and cellular expression of MGL was determined using IHC as visualized with fast red substrate. (A) Non-inflamed lung parenchyma of *Mtb* infected mouse at 8 week p.i. visualized with H&E, and (B) characterized by infrequent MGL+ cells. (C) Normal lung of non-infected mouse visualized with IHC that demonstrates infrequent although detectable MGL+ cells. (D) Organized area of inflammation due to *Mtb* infection at 8 weeks p.i. (E,F) IHC demonstrates MGL+ cells adjacent to lymphocyte aggregates of diffusely organized inflammatory foci. (G) MGL-1 and 2 expression on lung macrophages from disrupted lung tissue 8 weeks post-*Mtb* as assessed by flow cytometry (n=3). (H) MGL-1 expression on interstitial and (I) alveolar macrophages was assessed following 24 hours *in vivo Mtb* infection (n=3). The CLR MMR (CD206) was included due to its high expression on alveolar macrophages. Scale bars: 100 μm or 50 μm.

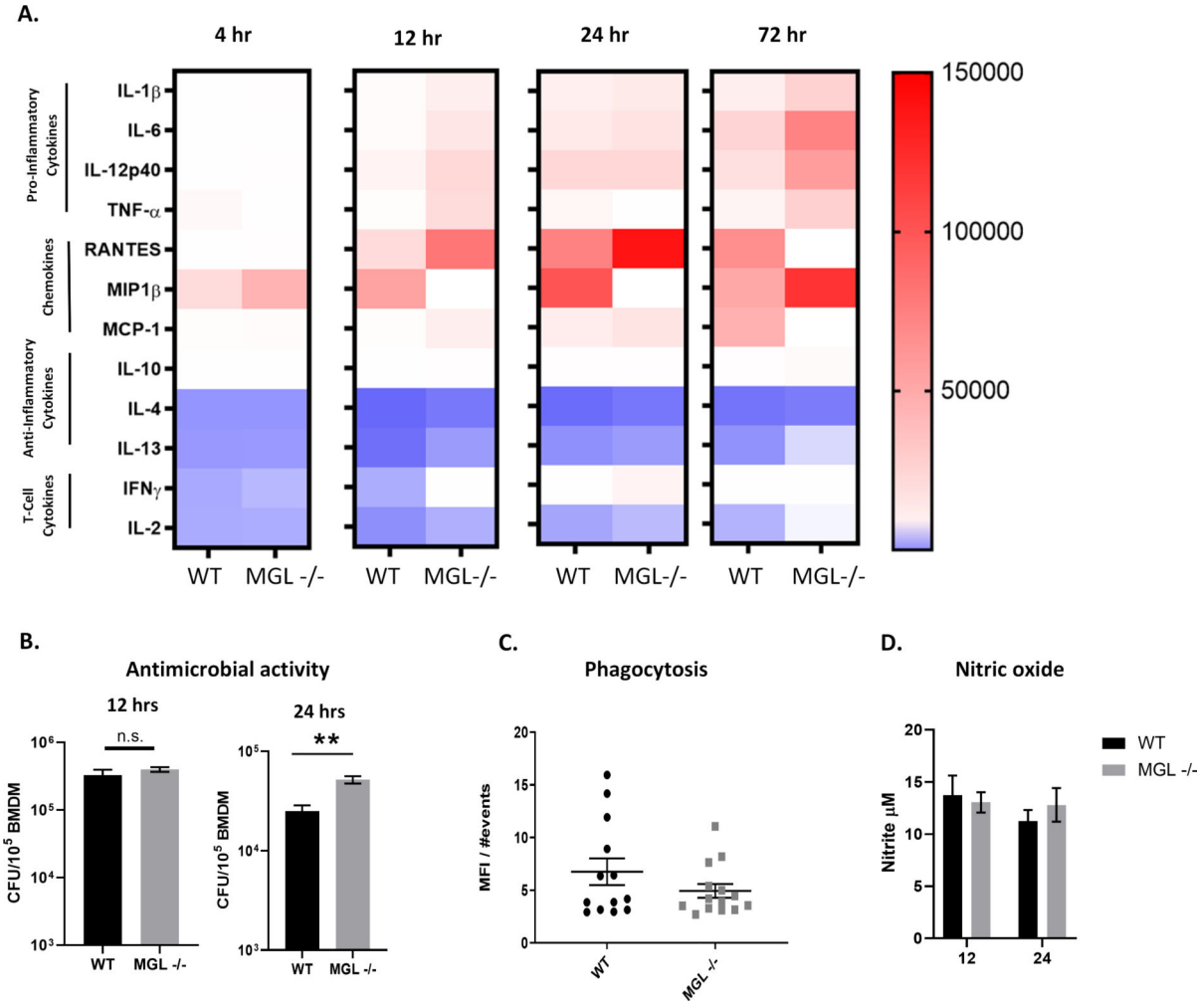

FIGURE 3. Impaired anti-mycobacterial and inflammatory signaling of MGL-1 deficient macrophages.

BMDMs from WT and MGL-1$^{-/-}$ mice were infected with 10 MOI *Mtb* H37Rv to determine differences in innate immune response and antimicrobial activity. (A) Inflammatory cytokine signatures of supernatants (n=3) measured with multiplex ELISA displayed as a relative change heatmap. (B) Intracellular mycobacterial burden 12 and 24 hours p.i. as determined by CFU enumeration (n=3). (C) Cellular uptake of CFSE labeled *Mtb* as determined by using flow cytometry at 2 hours p.i. (D) Production of NO as estimated with measurement of nitrite, 12 and 24 hours p.i (n=3). Statistical analysis was performed by Student's t-test. Differences compared to mock treatment are indicated with **p<0.01.

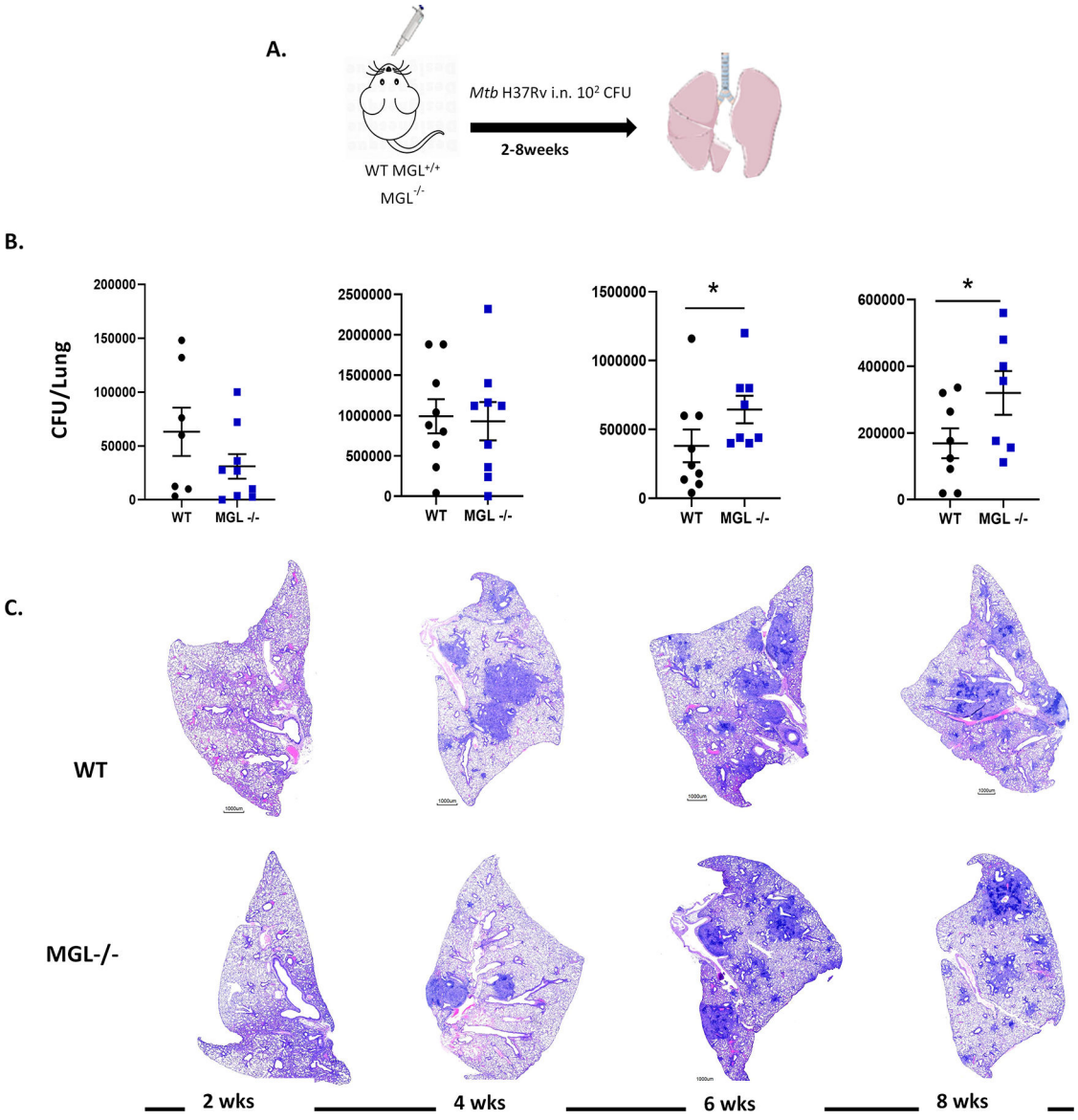

FIGURE 4. MGL-1-dependent regulation of mycobacterial burden *in vivo*.

(A) WT (MGL-$1^{+/+}$) and MGL-$1^{-/-}$ mice were infected with 10^2 CFU of *Mtb* H37Rv for 2, 4, 6, and 8 weeks. (B) Lung mycobacterial burden, and (C) representative lung histopathology of WT and MGL-$1^{-/-}$ mice (scale bar: 1000 μm). Groups of 7–9 animals in the WT and MGL-$1^{-/-}$ groups were used for analysis at each time point post-infection. Statistical analysis was performed using a Student's t-test. Significant differences between groups are indicated with *$p<0.05$.

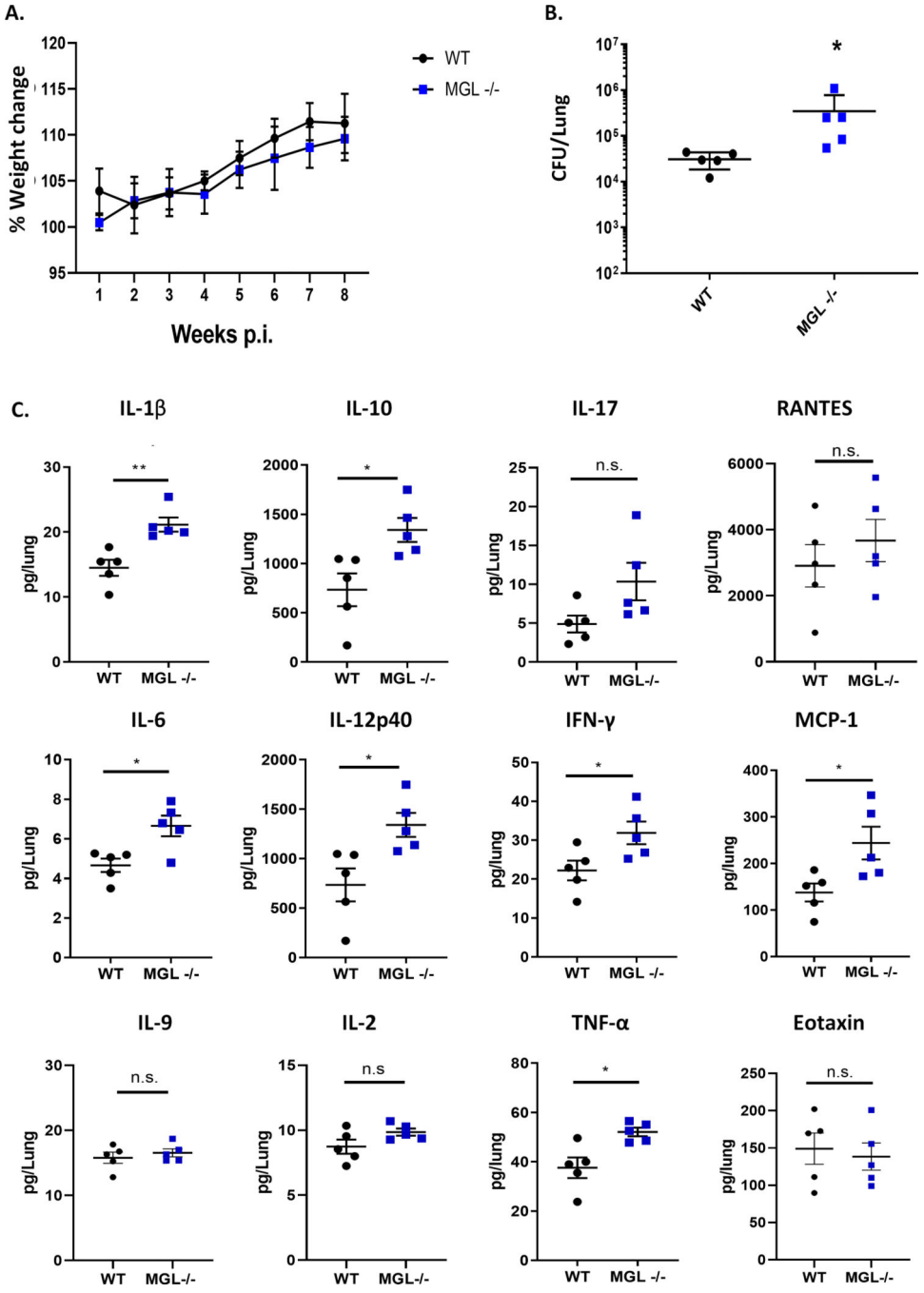

FIGURE 5. Inflammatory dysfunction due to *in vivo* loss of MGL-1.

Lung tissue from WT and MGL-$1^{-/-}$ mice (n=5) was harvested at 8 weeks p.i. with 10^2 *Mtb* H37Rv. (A) Percent weight change. (B) Homogenized lung tissue was assessed for bacterial load determined by CFU. (C) Multi-plex ELISA was used to determine cytokine and chemokine levels in supernatants of homogenized lung. Significant differences between groups are indicated with **p<0.01 and *p<0.05. Additional cytokine and chemokine results from the 23-plex analysis are shown in Supplemental Fig. 3.

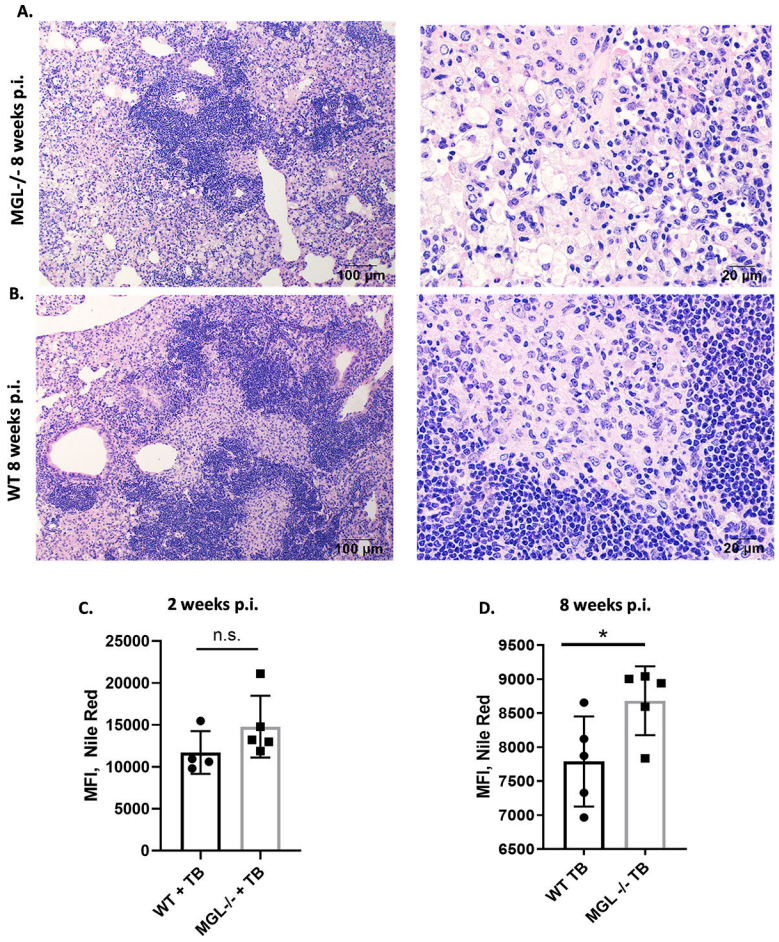

FIGURE 6. Accumulation of lipid rich cells in lungs of MGL-1-deficient mice.

Total lung leukocytes were isolated from lungs following 2 weeks (n=4–5) and 8 weeks (n=5) *Mtb* infection. (A, B) H&E sections of WT and MGL-1$^{-/-}$ lung tissue 8 weeks p.i. was analyzed by light microscopy for lipid rich cells. (C, D) Lipid rich cells were additionally stained with Nile red and quantified by flow cytometry analysis. Significant differences between groups are indicated with *p<0.05. Scale bars: 100 µm or 20 µm

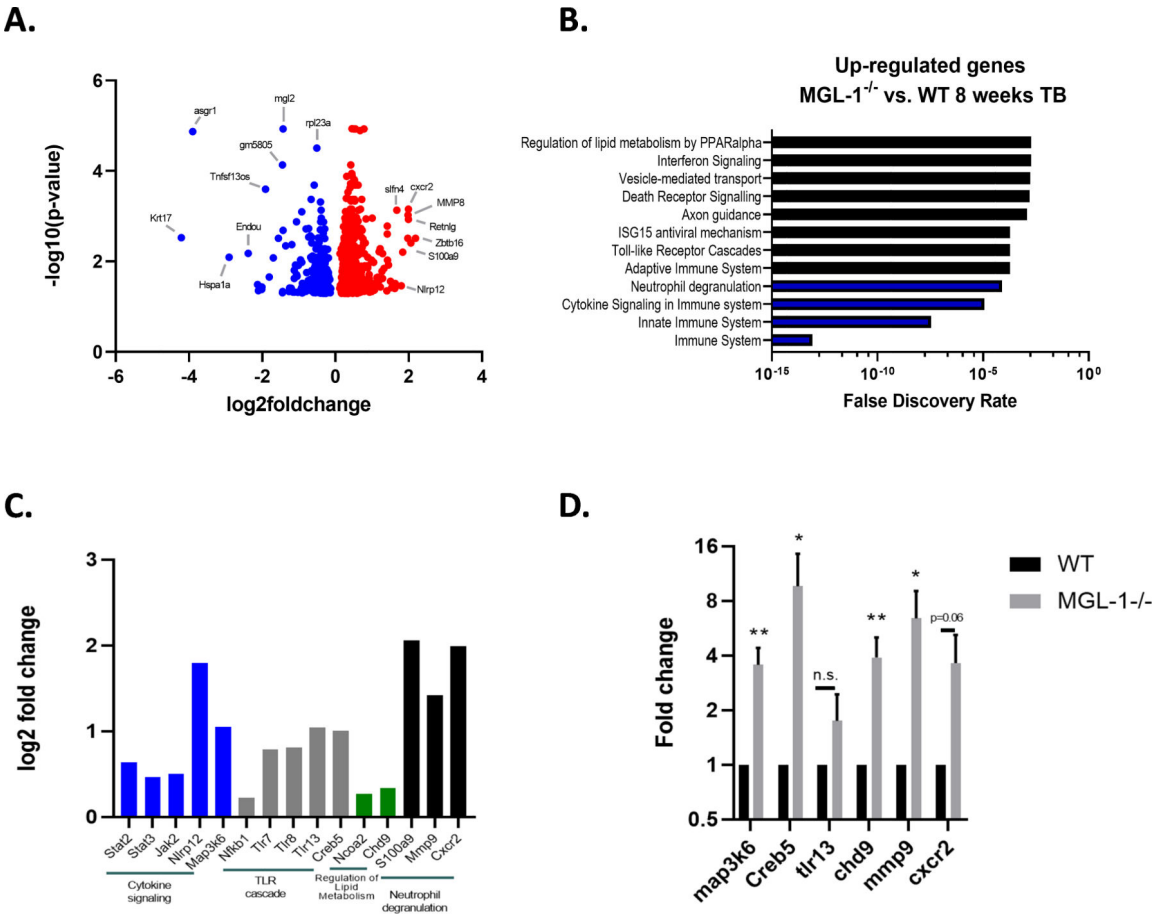

FIGURE 7. Differential gene expression due to MGL-1 deficiency.

WT and MGL-1$^{-/-}$ mice were infected with *Mtb* H37Rv for 8 weeks. Next generation RNA sequencing was performed on isolated lung tissue RNA (n=5). (A) Volcano plot of statistically significant (adj p-value ≤ 0.05) MGL-1$^{-/-}$ vs WT up-regulated and down-regulated genes. (B) Reactome pathway analysis of significant up-regulated genes. The top 12 pathways were selected based on false discovery rate. (C) Selected up-regulated genes representative of cytokine signaling, TLR cascade, regulation of lipid metabolism, and neutrophil degranulation pathways. (D) Up-regulated genes of interest were validated using q-PCR (n=5) in WT and MGL-1$^{-/-}$ lung tissue RNA. Differences compared to WT are indicated with **p<0.01, and *p<0.05.